Structural and Optical Properties of Two-Stage CuInSe₂ Thin Films Studied by Real Time Spectroscopic Ellipsometry

Dhurba R. Sapkota, Puja Pradhan, Prakash Koirala, Richard Irving, Adam B. Phillips, Randy J. Ellingson, Michael J. Heben, Sylvain Marsillac*, Nikolas J. Podraza, and Robert W. Collins

Wright Center for Photovoltaics Innovation & Commercialization, Univ. Toledo, Toledo, Ohio, 43606, USA; * Virginia Institute of Photovoltaics, Old Dominion Univ., Norfolk, Virginia, 23529, USA

Abstract — CuInSe₂ (CIS) thin films ~ 500-650 Å in thickness have been deposited on c-Si substrates by two-stage thermal coevaporation starting either from In₂Se₃ [according to In₂Se₃ + $(2Cu+Se) \rightarrow 2(CuInSe_2)$ or from $Cu_{2-x}Se$ [according to $Cu_2Se +$ $(2In+3Se) \rightarrow 2(CuInSe_2)$]. The design of such processes is facilitated by accurate calibrations of Cu and In₂Se₃ growth rates on substrate/film surfaces obtained by real time spectroscopic ellipsometry (RTSE). The two-stage deposited CIS films were also studied by RTSE to deduce (i) the evolution of film structure upon conversion of the starting In₂Se₃ or Cu_{2-x}Se films to CIS via Cu+Se or In+Se co-evaporation, respectively, and (ii) the complex dielectric functions of the starting films as well as the resulting CIS. The goal is to fabricate CIS that develops large grains as early as possible during growth for high quality materials in tandem solar cell applications. Results indicate that by depositing Cu_{2-x}Se in the first stage and exposing the film to In+Se flux in the second stage [as in the third stage of a threestage CIS process] well-defined bandgap critical points with no detectable subgap absorption are noted in films as thin as 650 Å.

Index Terms — optical variables measurement, ellipsometry, thin film devices, thickness measurement, photovoltaic cells.

I. INTRODUCTION

The first fully thin film CuInSe₂/CdS solar cell devices were fabricated from CuInSe₂ (CIS) absorber layers deposited by the co-evaporation of CuInSe₂ and Se, as reported in 1976 [1]. Further CIS research (subsequently extended to the related chalcopyrite alloys) was stimulated by the demonstration of a 9.4% CIS device by Mickelsen et al. in 1981 [2]. With single-junction solar cell efficiencies now increasing toward their Shockley-Queisser limits, the development of tandem or multi-junction solar cells is the next focus of attention with the goal to exceed the single-junction limits [3]. As a result of the recent interest in tandems, attention has returned to CIS due to its direct bandgap of 1.02 eV, which is among the narrowest of the direct bandgap thin film materials. The combination of a hybrid perovskite top cell and a CIS or low Ga content CuIn_{1-x}Ga_xSe₂ (CIGS) bottom cell has the potential for realizing high efficiency thin film tandems because of the excellent photovoltaic performance of devices based on these materials, their optimum bandgap pairings, and the thermal processing compatibility of the component solar cells.

Perovskite compounds were identified first as an efficient light harvester for photoelectrochemical cells and later work progressed from liquid to solid state junctions that enabled rapid increases in performance, reaching power conversion efficiencies > 24% in just 6 years [4-7]. Considering the high efficiencies achievable with low temperature processing, cells with perovskite absorbers can be deposited onto CIS devices without simultaneously annealing the window and transparent conductors deposited at low-temperature on the absorber. Furthermore, for the CIS junction of the tandem, the top contact and window layer can be selected for their electronic performance without the usual trade-off between open-circuit voltage and short-circuit current necessary for single junction cells. The high energy photons that are normally absorbed in the top contact transparent conductor and window layers of the single-junction CIS device are instead collected by the overlying perovskite cell of the tandem.

In this work, we introduce novel two-stage thermal coevaporation processes for CIS preparation, starting from either In₂Se₃ or Cu_{2-x}Se and completing with either Cu+Se or In+Se co-evaporation, respectively. For evaluation of these two approaches, CIS thin films ~ 500-650 Å thick were deposited on crystalline Si (c-Si) wafers at a substrate temperature of 570°C. All films were studied by real time spectroscopic ellipsometry (RTSE) during deposition to analyze the structural evolution as well as the optical properties after completion of each of the two stages. The reason for using c-Si substrates and thinner films than those in devices is to minimize the contributions of substrate-induced and growthinduced roughness on film surfaces. This enables higher sensitivity to thin film structural evolution and complex dielectric function spectra (ε_1 , ε_2) in RTSE analyses. In addition to determining the structural evolution of the starting films and the conversion of In₂Se₃ or Cu_{2-x}Se to CIS via Cu+Se or In+Se co-evaporation, respectively, the $(\varepsilon_1, \varepsilon_2)$ spectra of the starting films and resulting CIS provide information on grain size, defects, and phase composition. As a result, insights are obtained into optimization of processes leading to large grains as early as possible in these two-stage processes. The results are also relevant for understanding and optimizing the third stage of a three-stage deposition process for CIS. In the analogous, highly-successful three-stage process for the CIGS absorber of efficient solar cells, a thin layer of Cu_{2-x}Se on the CIGS surface is converted to Cu-poor CIGS upon exposure to In+Ga+Se flux in the third stage. The ultimate goal of this work is to obtain CIS of optimum stoichiometry and grain structure similarly, applying RTSE for calibration, monitoring, and control. Optimized CIS is to serve as the bottom cell absorber in tandem applications [8].

A. Evaporation Source Rates

For evaporation source calibrations, the thickness evolution for both the Cu and In₂Se₃ thin films has been obtained by RTSE. These films were deposited on native oxide covered c-Si wafers at room temperature and at 570°C, respectively, with evaporation source temperatures spanning the ranges of 1335-1395°C for Cu and 965-1025°C for In. For the In₂Se₃ calibration and for all two-stage depositions as well, the Se rate was set at 20 Å/s as measured by a quartz crystal monitor. Figures 1 and 2 show the structural evolution plotted versus accumulated deposition time for Cu and In₂Se₃, respectively. Step-wise increases in source temperature were applied during single Cu and In₂Se₃ depositions on the same substrate. A shutter was closed for 30 min during and after the setting of each source temperature to ensure stable rates before opening the shutter for deposition and for RTSE data collection at each step. RTSE analyses were performed on these data sets to determine the instantaneous deposition rates in the effective thickness, $d_{\text{eff}} = [(1-f_{vs}) d_s + d_b](1-f_{vb})$ which describes the volume of material per unit area, relevant for flux calibrations. Here, d_s is the surface roughness layer thickness, f_{vs} is the void volume fraction within the surface roughness layer, d_b is the bulk layer thickness, and f_{vb} is the volume fraction of voids in

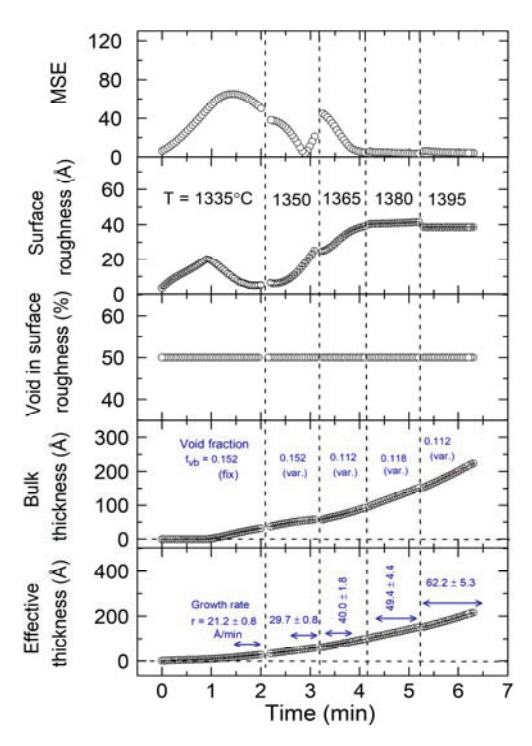


Fig. 1. Structural evolution of a Cu film deposited step-wise on a c-Si wafer at room temperature by evaporation using five different source temperatures as indicated. Shown are the mean square error of the fit (MSE), the surface roughness layer thickness d_s , the void content f_{vs} in the roughness layer (fixed at 50 vol.% for this deposition), the bulk layer thickness d_b , and the effective thickness d_{eff} , from which the deposition rate in terms of material volume/area is determined.

the bulk layer relative to the single crystal. Shown in the top four panels of Figs. 1 and 2 are the mean square error (MSE; a measure of the fit quality), d_s , the roughness void volume percent (100 vol.%) x f_{vs} (fixed for the Cu calibration), and d_b . Shown in the lowest panel is the key calibration result, the effective thickness of the film d_{eff} . For Cu, f_{vb} values are given along with d_b , whereas for In₂Se₃, f_{vb} is fixed at zero.

High MSEs can be observed in Fig. 1 for the two lowest Cu source temperatures. This occurs during the nucleation and coalescence when the $(\varepsilon_1, \varepsilon_2)$ spectra of Cu differ considerably from that of the bulk layer due to its plasmonic characteristics. The effective thickness rate also increases during nucleation and the most accurate results in Fig. 1 are obtained during the period of bulk layer growth. As a result, the calibration data for Cu at the lowest temperature is the least accurate. Plots of the effective thickness rates versus source temperature that illustrate the calibration approach are shown in Figs. 3 and 4 from the five-step Cu and In₂Se₃ depositions, respectively. Figure 3(b) presents the effective thickness rates of $Cu_{2-x}Se$ (x = 0, 0.2) obtained by using the growth rate of Cu shown in Fig. 3(a) as well as the crystal structure from Fig. 5 for x = 0and Ref. [9] for x = 0.2. It is preferable to calibrate Cu based on the growth of Cu_{2-x} Se of known x, according to the pseudobinary phase diagram; however, for this material, as well as for the less preferable calibration from pure In films, roughness evolution was too extensive for accurate analysis.

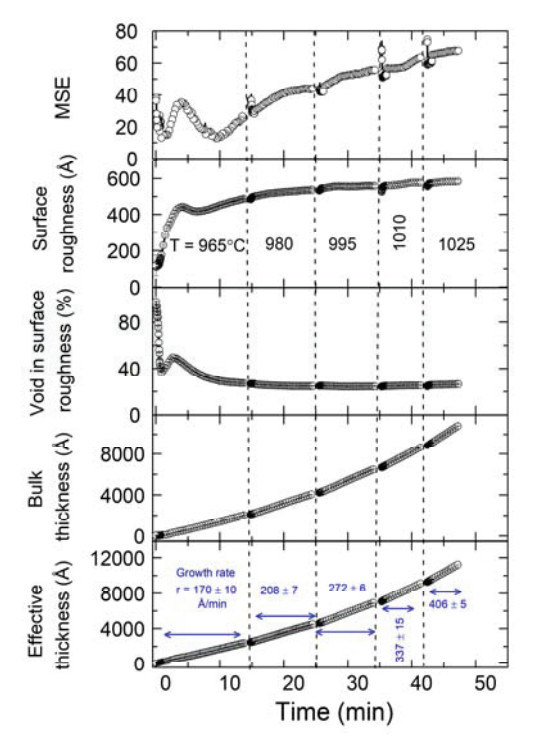


Fig. 2. Structural evolution of an In_2Se_3 film deposited step-wise on a c-Si wafer at 570°C by co-evaporation of In and Se using five different In source temperatures. Shown are the mean square error of the fit (MSE), the surface roughness layer thickness d_s , the void content f_{vs} in the roughness layer, the bulk layer thickness d_b , and the effective thickness d_{eff} , from which the material deposition rate in terms of volume/area is determined.

B. Calibration of CIS Deposition

An XRD analysis was performed on a Cu_{2-x}Se film deposited under the same conditions as the first stage of twostage CIS using a Cu source temperature of 1385°C and a Se rate of 20 Å/s. Shifts in the XRD peaks from those of the Cu₂Se reference (PDF# 97-004-1140) indicate strain, possibly due to Cu compositional deviations. Previous studies have shown that a wide range of flux ratios of Cu to Se favor $Cu_{2-x}Se$ with x = 0.20-25 [10]. The $Cu_{2-x}Se$ film exhibits an average crystallite size of ~ 145 Å, estimated as an average from the (111) and (220) peaks in Fig. 5 via the Scherrer equation. XRD and EDS analysis of In₂Se₃ was also performed, in this case for three individual depositions at source temperatures of 945°C, 970°C, and 990°C. The XRD pattern was found to be consistent with γ-In₂Se₃ (PDF# 97-000-1376) as shown in Fig. 6, with average grain sizes in the range $\sim 250-350$ Å from the (110) and (006) peaks (see Table I). From EDS, the films were found to be 0.5-0.8 at.% Se-rich with 67.2-67.5 at.% Se. Using the crystal structures of Cu, In₂Se₃, and CIS as well as the measured effective thickness rates by RTSE, the source temperature calibration shown in Fig. 7 could be obtained. This figure shows the pair of Cu and In source temperatures required to obtain CIS of a given Cu stoichiometry y = [Cu]/[In] (y = 0.8, 0.9, 1.0) and a given CIS deposition rate. Such a calibration is based on assumptions that the In₂Se₃ has the atomic concentrations (or mass density) of the single crystal, that the CIS lattice parameter does not change with stoichiometry over this range of y, and finally, that incoming metal precursors have unity sticking coefficient.

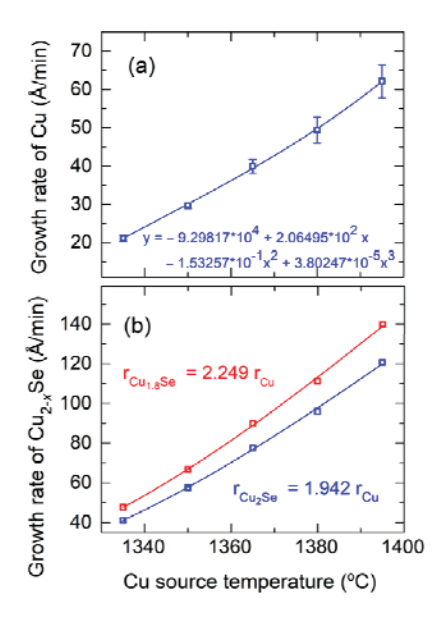


Fig. 3. (a) Effective thickness rate for Cu plotted versus the evaporation source temperature obtained from the RTSE data in Fig. 1. The data were collected in a single five-step deposition on c-Si at room temperature. (b) Predicted effective thickness rates of $Cu_{2-x}Se$ for x = 0 and 0.2 obtained from part (a) as well as from the crystal structure of $Cu_{2-x}Se$ based on XRD and Ref. [9], respectively.

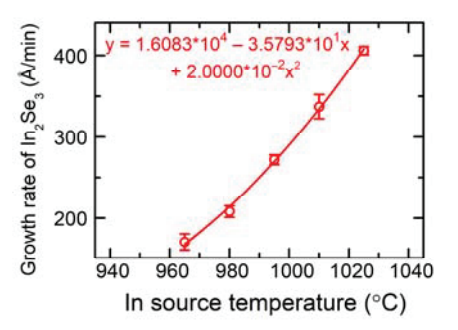


Fig. 4. Effective thickness rate for In_2Se_3 obtained from the analysis of RTSE data collected in a single five-step deposition on c-Si at 570°C using different In evaporation source temperatures.

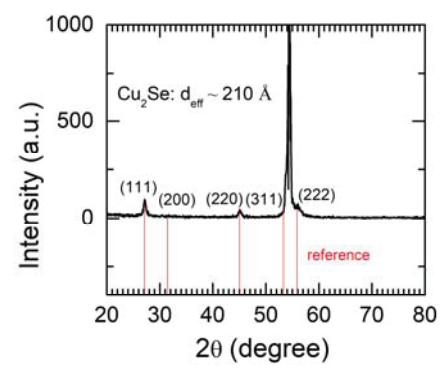


Fig. 5. X-ray diffraction (XRD) pattern for a $\text{Cu}_{2\text{-x}}\text{Se}$ film measured by a Rigaku instrument with small-angle X-ray scattering. The patterns were found to be consistent with Cu_2Se (berzelianite; PDF# 97-004-1140), but with a small shift from strain likely due to deviations from stoichiometric Cu_2Se .

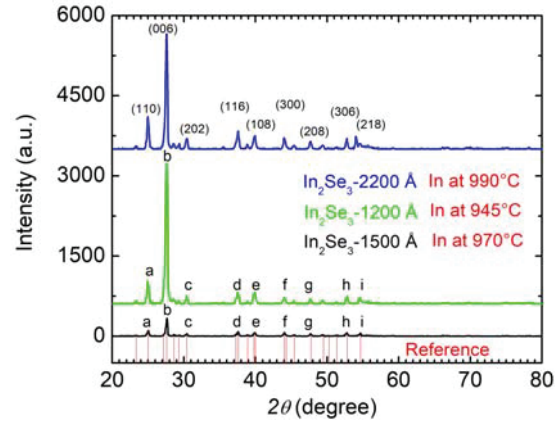


Fig. 6. XRD patterns measured as in Fig. 5 for a set of individual In_2Se_3 films deposited at different In source temperatures (see Table I). The patterns are consistent with the γ -phase (PDF# 97-000-1376).

TABLE I. EDS AND XRD RESULTS FOR THE In_2Se_3 FILMS OF FIG. 6 DEPOSITED AT DIFFERENT In SOURCE TEMPERATURES

| In source | In_2Se_3 | In | Se | In/Se | In ₂ Se ₃ grain |
|------------|---------------|---------|---------|-------|---------------------------------------|
| temp. (°C) | thickness (Å) | (at. %) | (at. %) | ratio | size (Å) |
| 945 | 1200 | 32.5 | 67.5 | 0.48 | 245 |
| 970 | 1500 | 32.8 | 67.2 | 0.49 | 370 |
| 990 | 2200 | 32.7 | 67.3 | 0.49 | 340 |

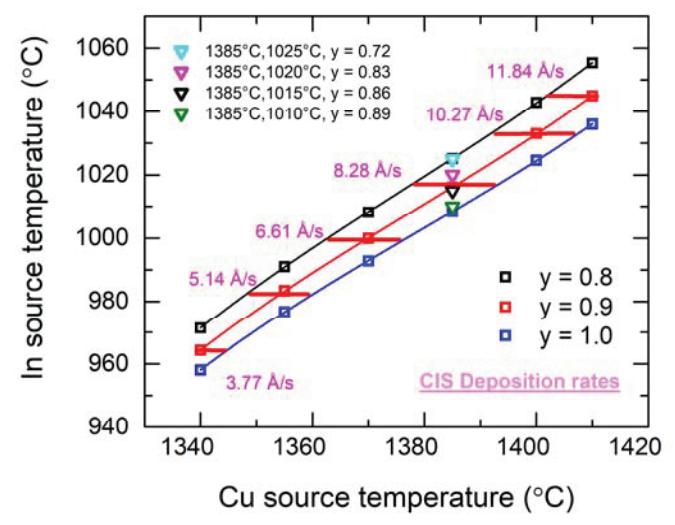


Fig. 7. Calibration curves for the source temperature settings used in the fabrication of CIS of different Cu stoichiometries y = [Cu]/[In] and different effective thickness rates. The four inverted triangles indicate a series of single-stage CIS depositions with Cu contents indicated. These results suggest a $y \sim 0.04$ -0.08 discrepancy which may arise due to deviations from assumptions made in calibration.

C. Two-stage CIS

Two different two-stage processes were explored for CIS. In the first, ~ 380 Å effective thickness of In_2Se_3 was deposited initially, and the resulting film was exposed to Cu and Se flux for ~ 0.73 min according to $In_2Se_3 + (2Cu + Se) \rightarrow 2(CuInSe_2)$. This is analogous to the second stage of a three-stage CIGS deposition. In the second two-stage process, ~ 150 Å effective thickness of $Cu_{2-x}Se$ is deposited, and then the film is exposed to In and Se flux for ~ 1.3 min according to $Cu_2Se + (2In + 3Se) \rightarrow 2(CuInSe_2)$. This is analogous to the third stage of three-stage CIGS deposition. The substrate temperature was 570°C for the two stages of each process.

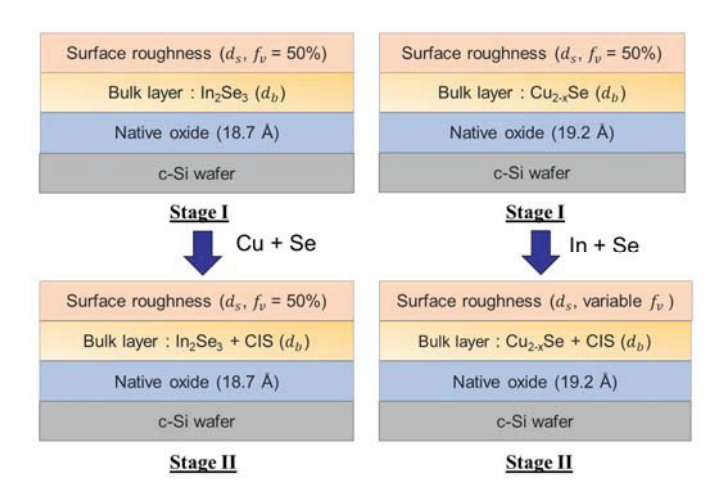


Fig. 8. Structural model used in analyses of RTSE data for the two-stage CIS deposition processes starting from In₂Se₃ (left) and from Cu_{2-x}Se (right). In the second stage, the bulk layer is modeled as a composite with the Bruggeman effective medium approximation.

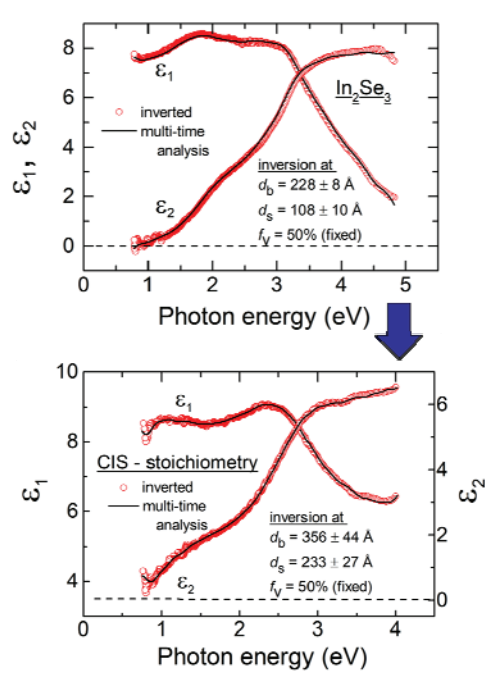


Fig. 9. Complex dielectric functions (ϵ_1 , ϵ_2) for two-stage deposition of CIS on c-Si at 570°C starting from In_2Se_3 (top), followed by exposure to Cu + Se flux to generate stoichiometric CIS (bottom). For these two-stage CIS thin films, multi-time analysis of RTSE data was performed (lines), which was then corroborated by numerical inversion (points). The (ϵ_1 , ϵ_2) spectra were used to generate the structural evolution in the two different stages as shown in Fig. 11.

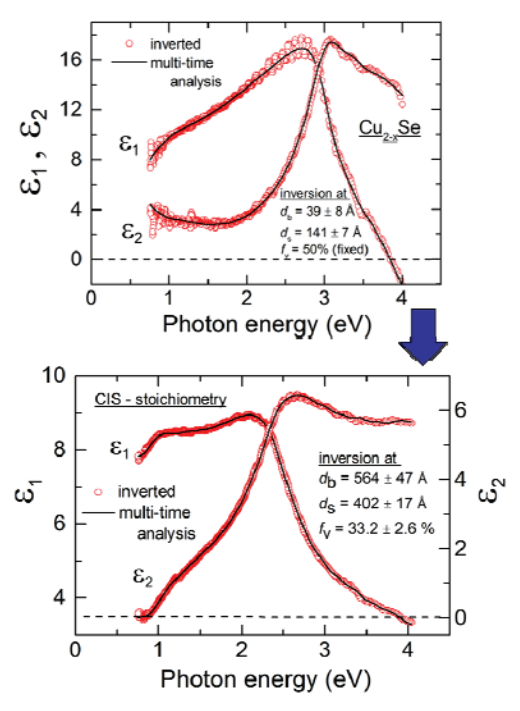


Fig. 10. Complex dielectric functions (ϵ_1 , ϵ_2) for two-stage deposition of CIS on c-Si at 570°C starting from Cu_{2-x}Se (top) followed by exposure to In + Se flux to generate stoichiometric CIS (bottom). For these results, multi-time analysis was performed (lines) as in Fig. 9, which was then corroborated by inversion (points). These (ϵ_1 , ϵ_2) spectra were used to generate the structural evolution in Fig. 12.

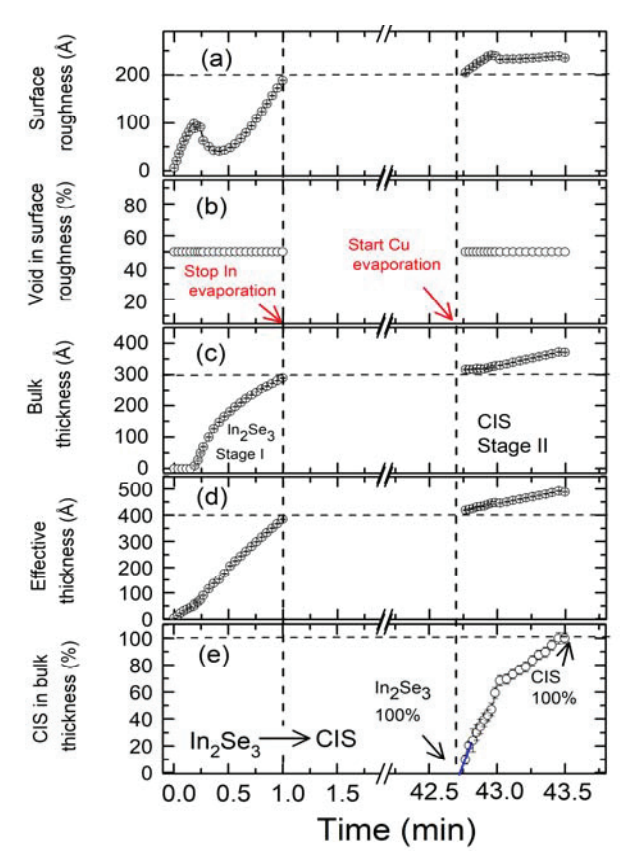


Fig. 11. RTSE analysis results for two-stage deposition of CIS on c-Si at 570°C starting from In_2Se_3 , followed by exposure to Cu + Se flux. Panels include the (a) surface roughness layer thickness d_s ; (b) void content in the roughness layer f_{vs} , fixed at 50 vol.%; (c) bulk layer thickness d_b ; (d) effective thickness $[d_{eff} = d_b + (1-f_{vs})d_s]$; and (e) CIS content in the bulk $(In_2Se_3 + CIS)$ layer.

III. RESULTS AND DISCUSSION: RTSE ANALYSIS OF $CuInSe_2$ FABRICATED IN TWO-STAGE PROCESSES

Figure 8 shows the structural/optical models used to analyze the RTSE data collected during the deposition of CIS in the two-stage processes on c-Si substrates held at a temperature of 570°C. The left and right panels of Fig. 8 show the processes starting from In_2Se_3 and $Cu_{2-x}Se$, respectively. The y=1.0 composition in the analysis is identified through the (ϵ_1, ϵ_2) spectra of the evolving layers. Figures 9 and 10 present the resulting spectra of the starting materials In_2Se_3 and $Cu_{2-x}Se$, respectively, along with those of the final stoichiometric CIS layers. These spectra were obtained by multi-time analysis corroborated by numerical inversion.

Figure 11 shows the structural evolution of the film starting from the onset of In_2Se_3 deposition and during conversion to CIS upon exposure to Cu + Se. A ~ 40 min gap is evident in the time scale between the results obtained at the end of the In_2Se_3 deposition and those obtained upon the initial conversion to CIS. This gap occurs due to a substrate shutter which blocks the RTSE probe in the change-over from In flux to stable Cu flux. Also, the small gap in the data at the onset of Cu flux occurs due to the opening of a shutter which blocks

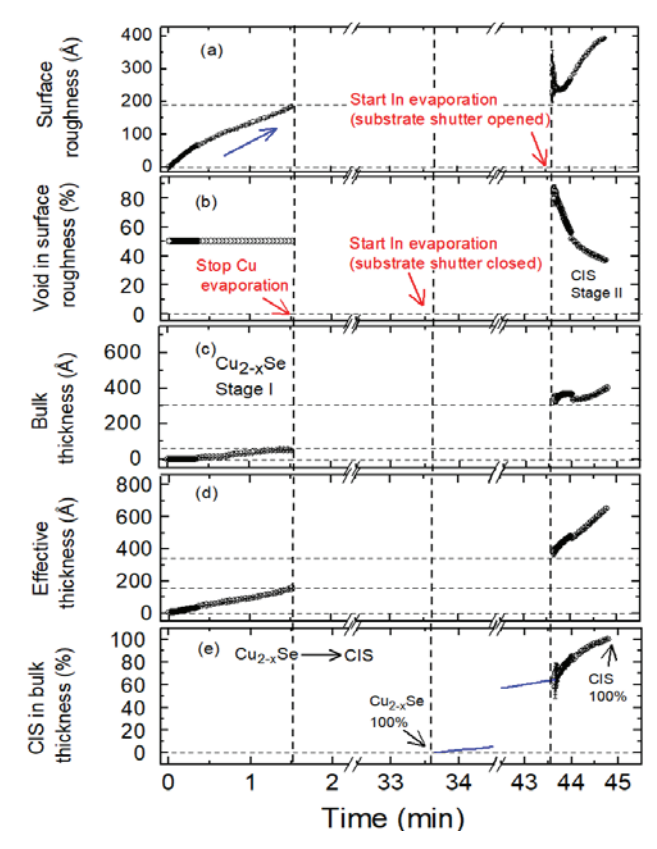


Fig. 12. RTSE analysis results for two-stage deposition of CIS on c-Si at 570°C starting from $Cu_{2-x}Se$, followed by exposure to In + Se flux. Panels include the (a) surface roughness layer thickness d_s ; (b) void content in the surface roughness layer f_{vs} ; (c) bulk layer thickness d_b ; (d) effective thickness $[d_{eff} = d_b + (1 - f_{vs})d_s]$; and (e) CIS content in the bulk $(Cu_{2-x}Se + CIS)$ layer.

TABLE II. SUMMARY OF THE GROWTH RATE OF TWO-STAGE CIS THIN FILMS STUDIED WITH RTSE

| CIS process | Growth rate in stage I | CIS growth rate in stage II | Final effective thickness | Endpoint y = [Cu]/[In] |
|---|---------------------------|-----------------------------|---------------------------------|------------------------------|
| Two-stage starting from In ₂ Se ₃ | 354 ± 6 Å/min | 100 ± 10 Å/min | $489 \pm 3 \text{ Å}$ | 1.0 |
| Two-stage starting from Cu _{2-x} Se | 90 ± 10 Å/min | 256 ± 12 Å/min | 648 ± 2 Å | 1.0 |

the RTSE probe. In addition to missing data due to the blockage by the shutter, some incorporation of Cu occurs while the shutter is closed since the shutter does not completely prevent incoming Cu + Se flux from reaching the In₂Se₃ film surface. As a result of these two effects, the equivalent of ~ 10 vol.% In₂Se₃ has been converted before the first usable RTSE time point. The In₂Se₃ is deposited in stage I to the effective thickness of ~ 380 Å. In this process, the film proceeds through a nucleation stage whereby the surface roughness first increases to ~ 100 Å and then coalesces to a

thickness of ~ 40 Å, before increasing again to a thickness of ~ 190 Å. The growth rates of In_2Se_3 in stage I and CIS in stage II stabilize at values of 354 Å/min and 100 Å/min, respectively, as presented in Table II. The final effective thickness of stoichiometric CIS at the endpoint is 489 Å.

Figure 12 shows the corresponding results starting from the onset of Cu_{2-x}Se deposition. In this case, as for the deposition of Fig. 11, $a \sim 40$ min gap is evident in the time scale between the stages. In the flux stabilization time, deposition occurs on the substrate surface behind the shutter to an extent depending on the vapor pressure of the metal. The effect is small for the change-over from In to Cu whereas for the change-over from Cu to In, considerable In and Se exposure of the surface occurs while the shutter is closed. It is estimated that ~ 70 vol.% Cu2-xSe has been converted to CIS before the first usable RTSE time point. For the first ~ 25 seconds of Cu_{2-r}Se deposition, a one-layer model is applied during which time the surface roughness thickness increases to ~ 70 Å. Upon growth of the bulk layer, no coalescence effect is observed and the roughness layer grows at a considerably faster rate than the bulk layer. For a liquid-like material such as Cu_{2-x}Se, this effect may be due to a continuous ripening of clusters whereby smaller clusters combine into larger ones as growth proceeds. The result in this case, is a bulk layer thickness of ~ 50 Å and a roughness layer thickness ~ 180 Å. The effective thickness increases linearly with time at a rate of 90 Å/min as given in Table II, much slower than the corresponding rate of In₂Se₃ during the first stage of the alternative two-stage process in Fig. 11. The final effective thickness of Cu_{2-x}Se is ~ 150 Å as noted in Fig. 12.

A comparison of Figs. 11 and 12 is of interest in evaluating the two-stage processes. First, it is observed that at the end of the first stages of In_2Se_3 and $Cu_{2-x}Se$, the surface roughness thickness values are similar, $\sim 190~\text{Å}$. In spite of this, the structural evolution of the first stage films is different such that In_2Se_3 undergoes a nucleation-coalescence sequence whereas $Cu_{2-x}Se$ undergoes continuous roughening. Upon conversion to CIS, the deposition starting from In_2Se_3 shows only weak roughening to a thickness of $\sim 240~\text{Å}$, whereas that starting from $Cu_{2-x}Se$ shows strong roughening to $\sim 400~\text{Å}$, typical of the growth of large grains. This interpretation is supported by a sharp $E_0(A,B)$ bandgap onset in the $(\epsilon_1,\ \epsilon_2)$ spectra with no detectable sub-gap absorption, and a more clearly defined $E_1(A)$ critical point in ϵ_2 near 2.6 eV for the CIS deposition starting from $Cu_{2-x}Se$.

V. CONCLUSIONS AND FUTURE WORK

Films of CuInSe₂ ranging in thickness from ~ 500 Å to 650 Å have been deposited on Si wafer substrates at 570°C in novel two-stage co-evaporation processes. The structural evolution and the complex dielectric functions (ϵ_1 , ϵ_2) at the stoichiometric endpoint of the films are obtained by real time and in situ spectroscopic ellipsometry. One two-stage process explored here starts with an In₂Se₃ deposition and is followed by Cu+Se exposure, the latter yielding stoichiometric CIS at

the endpoint. The other two-stage process starts with $Cu_{2-x}Se$ deposition and is followed by In+Se exposure to reach the CIS endpoint. This second process starting from $Cu_{2-x}Se$ shows features in the structural evolution and $(\varepsilon_1, \varepsilon_2)$ spectra that are consistent with the growth of large CIS crystallites during the second stage, yielding an endpoint suitable for forming a solar cell junction. These features include rapid second stage roughening and $(\varepsilon_1, \varepsilon_2)$ spectra having sharp critical points.

Future efforts will focus on integrating two and three stage processes into CIS solar cell fabrication. It is anticipated that this will serve as a suitable starting point for high efficiency CIS solar cells which are also expected to require further absorber process enhancements. These may include post-deposition alkali metal treatments as well as introduction of Ga near the back contact to generate a device suitable for the bottom cell of a polycrystalline tandem solar cell.

ACKNOWLEDGEMENT

This research is supported by NSF Award EECS-1665172.

REFERENCES

- [1] L. Kazmerski, F. White, and G. Morgan, "Thin-film CuInSe₂/CdS heterojunction solar cells," *Appl. Phys. Lett.*, vol. 29, pp. 268-270, 1976.
- [2] R. Mickelson and W. Chen, "Development of a 9.4% efficient thin-film CuInSe₂/CdS solar cell," *Proc. 15th IEEE Photovoltaic Specialists Conference*, pp. 800-804, 1981.
- [3] W. Shockley and H. J. Queisser, "Detailed balance limit of efficiency of p-n junction solar cells," *J. Appl. Phys.*, vol. 32, pp. 510-519, 1961.
- [4] A. Kojima, K. Teshima, Y. Shirai, and T. Miyasaka, "Organometal halide perovskites as visible-light sensitizers for photovoltaic cells," *J. Am. Chem. Soc.*, vol. 131, pp. 6050-6051, 2009.
- [5] M. Lee, J. Teuscher, T. Miyasaka, T. Murakami, and H. J. Snaith, "Efficient hybrid solar cells based on meso-superstructured organometal halide perovskites," *Science*, vol. 338, pp. 643-647, 2012.
- [6] T. Feurer, B. Bissig, T. P. Weiss, R. Carron, E. Avancini, J. Löckinger, S. Buecheler, and A. N. Tiwari, "Single-graded CIGS with narrow bandgap for tandem solar cells," *Sci. Technol. Adv. Mater.*, vol. 19, pp. 263-270, 2018.
- [7] Q. Han, Y. Hsieh, L. Meng, J. Wu, P. Sun, E. Yao, S. Chang, S. Bae, T. Kato, V. Bermudez, and Y. Yang, "High-performance perovskite/Cu(In,Ga)Se₂ monolithic tandem solar cells," *Science*, vol. 361, pp. 904–908, 2018.
- [8] R. H. Ahangharnejhad, A. B. Phillips, K. Ghimire, P. Koirala, Z. Song, H. M. Barudi, A. Habte, M. Sengupta, R. J. Ellingson, Y. Yan, R. W. Collins, N. J. Podraza, and M. J. Heben, "Irradiance and temperature considerations in the design and deployment of high annual energy yield perovskite/CIGS tandems," *Sustain. Ener. Fuels*, 2019; DOI: 10.1039/C9SE00237E.
- [9] N. N. Bikkulova, S. A. Danilkin, H. Fuess, E. L. Yadrovskii, A. I. Beskrovnyi, A. N. Skomorokhov, Z. A. Yagafarova, and G. N. Asylguzhina, "Crystal structure of non-stoichiometric copper selenides studied by neutron scattering and X-ray diffraction," *Crystal. Rep.*, vol. 48. pp. 370-373, 2003.
- [10] J. Walker, H. Khatri, S. Little, V. Ranjan, R. Collins, and S. Marsillac, "Optical and physical characterization of Cu_{2-x}Se thin films for real time spectroscopic ellipsometry on Cu(In,Ga)Se₂-based photovoltaic devices", *MRS Proc.*, vol. 1210, 1210-Q06-02: 1-6.